REVIEW

Check for updates

Inorganic planar π-conjugated groups in nonlinear optical crystals: review and outlook

Pifu Gong, [ID] [a] Xiaomeng Liu,[a,b] Lei Kang[a] and Zheshuai Lin [ID] *[a,b,c]

Nonlinear optical (NLO) materials have been playing significant roles in laser science and technology for converting laser wavelengths to spectral regions where normal lasers operated poorly. Inorganic planar π-conjugated groups possessing both large second harmonic generation (SHG) responses and optical anisotropy are one of the most desirable fundamental building units (FBUs) for NLO materials. Up to now, inorganic planar π-conjugated groups including $[BO_3]$, $[B_3O_6]$, $[CO_3]$, $[NO_3]$, $[H_xC_3N_3O_3]$ (x varying from 0 to 3), $[BS_3]$, $[B_3S_6]$, $[HgSe_3]$, $[AgSe_3]$, and $[B_2P_5]$ units are reported as NLO-active groups, which strongly enhance the structural diversity of NLO materials. In this review, the NLO materials containing inorganic planar π-conjugated groups are classified according to their shortest transparent regions, *i.e.* deep-ultraviolet (DUV, $\lambda < 200$ nm), ultraviolet (UV, 200 nm $< \lambda < 380$ nm), visible (VIS, 380 nm $< \lambda < 780$ nm), and infrared (IR, $\lambda > 780$ nm) regions. On the basis of available experimental and calculated data, the structure–property relationships and potential applied wave ranges for different inorganic planar π-conjugated groups are discussed.

Introduction

As important photoelectric functional materials, nonlinear optical (NLO) crystals have played unique roles in laser frequency conversion technology, which can efficiently expand the spectral regions of common laser sources.[1] Owing to their excellent per- formances, NLO crystals in all-solid-state laser systems have been widely applied in industrial processing, semiconductor manufacturing, photolithography, military confrontation, noninvasive medical diagnostics and signal communications.[2–5] After making continuous effort for decades, many useful NLO crystals, such as $KBe_2BO_3F_2$ (KBBF), β-BaB_2O_4 (BBO), LiB_3O_5 (LBO), $KTiOPO_4$ (KTP), $AgGaS_2$ (AGS), *etc.* have been developed and applied for laser frequency conversion in the deep ultraviolet (DUV), ultraviolet (UV), visible (VIS) and infrared (IR) regions.[6–11] Meanwhile, great progress has been made on the research of structure–property relationships, which reveal the deterministic effects of the NLO-active units on the NLO performances.[12–17]

[a]Technical Institute of Physics and Chemistry, Chinese Academy of Sciences, Beijing 100190, PR China. E-mail: zslin@mail.ipc.ac.cn
[b]University of the Chinese Academy of Sciences, Beijing 100049, PR China
[c]Center of Materials Science and Optoelectronics Engineering, University of Chinese Academy of Sciences, Beijing 100049, PR China

Pifu Gong received his B.S. in Physics from Shandong Normal University and then obtained his Ph.D. in Condensed Matter Physics from Technical Institute of Physics and Chemistry (TIPC), Chinese Academy of Sciences (CAS) in 2017. His current research focuses on developing new nonlinear-optical materials.

Pifu Gong

Zheshuai Lin obtained his Ph.D. from Fujian Institute of Research on the Structure of Matter, CAS, in 2002. Since 2008, he has been working as a professor at TIPC, CAS. His research into non- linear-optical crystals employs a variety of modeling techniques spanning analytical and quantum mechanics.

Zheshuai Lin

To realize laser frequency conversion, a NLO crystal must satisfy several fundamental but rigorous requirements, including a wide transparent window for an operating wave range, large second harmonic generation (SHG) response, and sufficient birefringence to achieve phase matching.[18,19] All of them are closely related to the fundamental building units (FBUs). On the basis of structure–property relationships, planar π-conjugated groups, second-order Jahn–Teller (SOJT) distorted $[MQ_6]$ (M = Ti, Nb, Ta, Mo, W, Te, *etc.*; Q = O, S, Se, Te) groups, distorted polyhedra centered by stereochemically active long pair (SALP) cations (Pb, Bi, Sb, I, *etc.*), rare-earth cation centered polyhedra, and metal element centered $[MQ_4]$ (M = Zn, Al, In, Ga, Ge, *etc.*; Q = O, S, Se, Te) tetrahedra are regarded as NLO-active units.[20–23] Among them, the planar π-conjugated groups with large SHG responses and optical anisotropy are one of the most desirable FBUs for NLO materials and many materials have achieved practical laser frequency conversion in DUV and UV regions using these groups.

Up to now, the reported planar π-conjugated NLO-active groups include $[BO_3]$, $[B_3O_6]$, $[CO_3]$, $[NO_3]$, $[H_xC_3N_3O_3]$ (x varying from 0 to 3), $[BS_3]$, $[B_3S_6]$, $[HgSe_3]$, $[AgSe_3]$, and $[B_2P_5]$ units. $[BO_3]$ and $[B_3O_6]$ possessing π_4^3 and π_9^9 configurations (where the subscript is the number of atoms constructing the π-conjugated group and the superscript is the number of π-electrons constructing the π-orbitals), respectively, are the most common FBUs for DUV and UV NLO borates. In 2018, Prof. Zhao reviewed the role of cations in $[BO_3]$-based NLO materials and Prof. Pan provided a comprehensive review of fluorooxoborates, which provide a better understanding of the structure–property relationships in NLO borates.[24,25] $[CO_3]$ (π_4^4) and $[NO_3]$ (π_4^5) have similar structural configurations to $[BO_3]$, but provide more π electrons on the delocalized π orbitals, which results in larger SHG responses. Our group also systematically reviewed the NLO carbonates and nitrates and investigated the relationship between the SHG responses and the arrangements of the planar π-conjugated NLO-active groups inside.[26,27] In 2017, our group pointed out that the $[H_xC_3N_3O_3]$ (π_9^9) groups could serve as NLO-active units for their similar electronic and structural configuration to the $[B_3O_6]$ units.[28] After that, dozens of hydro-cyanurates and cyanurates are reported, which strongly promote the development of related fields.[29–32] Very recently, the no-oxygen-containing planar π-conjugated units, *i.e.* $[BS_3]$ (π_4^3), $[B_2S_6]$ (π_9^9), $[HgSe_3]$ (π_4^2), $[AgSe_3]$ (π_4^1), and $[B_2P_5]$ (π_7^5), have been reported as NLO-active units and have attracted much attention in the exploration of related IR NLO materials. All these reported planar π-conjugated NLO-active groups can achieve both large SHG responses and optical anisotropy, which make them the most desirable FBUs for NLO materials.

Although some reviews have been reported for certain kinds of planar π-conjugated groups, a systematic review covering all the planar NLO-active groups is absent.[33–36] In this work, all the kinds of inorganic planar π-conjugated groups are covered and the related NLO materials are classified according to their shortest transparent regions, *i.e.* deep-ultraviolet (DUV, λ < 200 nm), ultraviolet (UV, 200 nm < λ < 380 nm), visible (VIS,

380 nm < λ < 780 nm), and infrared (IR, λ > 780 nm) regions. On the basis of available experimental and calculated data, the potential applied wave ranges for different inorganic planar π-conjugated groups are investigated. In addition, the structure–property relationships and further developments of the NLO materials containing planar π-conjugated groups are discussed.

2. DUV transparent NLO crystals containing planar π-conjugated groups

According to our survey, only the NLO materials with $[BO_3]$, $[B_3O_6]$, $[CO_3]$ and $[NO_3]$ units possess the property of DUV transparency. In this section, the structures and main optical properties of the related DUV transparent NLO crystals are discussed based on their planar π-conjugated groups.

2.1 DUV transparent borate with planar $[BO_3]$ and $[B_3O_6]$ units

The $ABe_2BO_3F_2$ (A = Na, K, Rb, Cs, NH₄, Tl) family is a classical series of NLO materials. To date, $KBe_2BO_3F_2$ (KBBF) is still the solo practically usable DUV NLO crystal to generate coherent light shorter than 200 nm by a direct frequency doubling method. This unique ability is attributed to its short UV cutoff edge (146 nm), large SHG coefficient (d_{11} = 0.47 pm V^{-1}), and moderate birefringence (0.088 at 400 nm). However, KBBF suffers a strong layering growth tendency for the weak F⁻–K⁺ electrostatic attraction between the adjacent $[Be_2BO_3F_2]_\infty$ layers, which strongly hinders its commercialization. To enhance the interlayer forces, NH₄⁺ cations are introduced to replace the K⁺ cations in KBBF. $NH_4Be_2BO_3F_2$ (ABBF) possesses the same structure as KBBF, but introduces the hydrogen bonds between the layers.[37] As per analysis, ABBF exhibits comparable optical properties to KBBF, such as a short UV cutoff edge (153 nm), large SHG response (1.2 times that of KH_2PO_4, *i.e.* 1.2 × KDP), and moderate birefringence (0.078 at 400 nm). Ultimately, when A-site cations are cut off to overcome the layering tendency of KBBF, γ-Be_2BO_3F (γ-BBF) was obtained. γ-BBF crystallizes in the non-centrosymmetric (NCS) trigonal space group $R32$.[37] Its powder SHG response is found to be 2.3 times that of KDP. To evaluate its bandgap and birefringence, first-principles calculations are performed and the results reveal that γ-BBF possesses a large bandgap (about 8.56 eV), a moderate birefringence (0.105 at 532 nm), and a large SHG coefficient (d_{11} = 0.67 pm V^{-1}). According to the refractive index dispersion equations, the calculated shortest phase matching edges for ABBF and γ-BBF are 173.9 nm and 146 nm, respectively. Therefore, both ABBF and γ-BBF can be used as new DUV NLO materials (Fig. 1).

$Li_4Sr(BO_3)_2$ crystallizes in the monoclinic NCS space group Cc.[38] As shown in Fig. 2, its structure is composed of 2D $[SrBO_3]_\infty$ layers (Fig. 2b), which are further bridged by $[BO_3]$ units to construct the 3D framework of $Li_4Sr(BO_3)_2$. Based on the grown single crystal (Fig. 2c), the UV cutoff edge is found
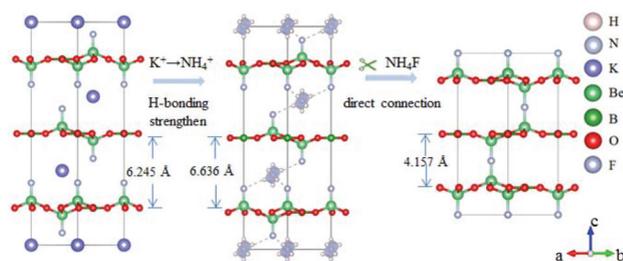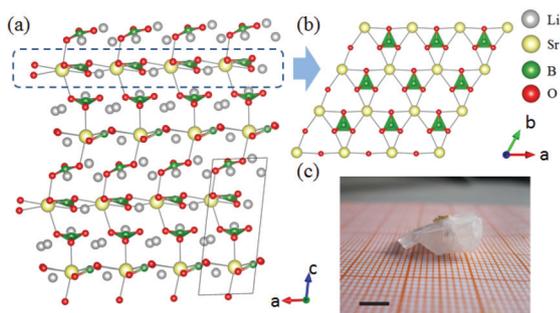
Fig. 1 Structural evolution from KBBF, ABBF to γ-BBF.

Fig. 2 (a) The crystal structure, (b) the [SrBO$_3$] layer, and (c) the as-grown crystal for Li$_4$Sr(BO$_3$)$_2$.

to be 186 nm (corresponding to the bandgap of 6.69 eV). The powder SHG response is found to be 2 times that of KDP. According to the calculated results, Li$_4$Sr(BO$_3$)$_2$ has a large SHG coefficient of 0.64 pm V^{-1} (d_{12}) and a birefringence of 0.056 (at 532 nm), which agree well with the experimental results. Therefore, Li$_4$Sr(BO$_3$)$_2$ is an attractive candidate for UV NLO applications.

NH$_4$B$_4$O$_6$F is the first member of AB$_4$O$_6$F (A = NH$_4$, Na, K, Rb, Cs) series NLO crystals.[39–42] The compound crystallizes in the polar NCS space group *Pna*2$_1$. As shown in Fig. 3, three [BO$_3$] and one [BO$_3$F] connect together by sharing the O atoms to form the FBU of NH$_4$B$_4$O$_6$F. These FBUs further construct the 2D [B$_4$O$_6$F]$_\infty$ layers extended along the *a–c* plane with the NH$_4^+$ cations inserted in the space between the layers. As shown by optical measurements, NH$_4$B$_4$O$_6$F exhibits a wide DUV transparent range down to 156 nm (corresponding to the
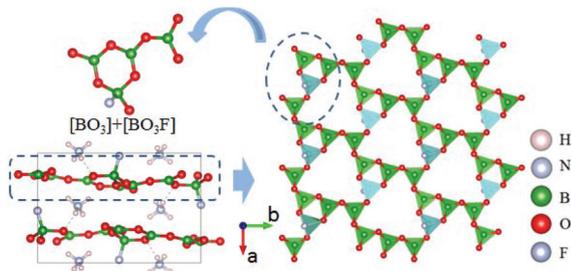
bandgap of 7.97 eV) and suitable birefringence (0.130 at 407 nm) that enable frequency doubling to 158 nm. The SHG response is found to be 2.5 times that of KDP. The calculated SHG coefficient (d_{33} = −1.19 pm V^{-1}) and birefringence (0.117 at 1064 nm) show good agreement with the experimental results. All these properties clearly demonstrate that NH$_4$B$_4$O$_6$F is an important NLO crystal for DUV applications.

CsB$_4$O$_6$F also belongs to the AB$_4$O$_6$F (A = NH$_4$, Na, K, Rb, Cs) series NLO crystals, but has a different structural type compared to NH$_4$B$_4$O$_6$F.[40] The compound crystallizes in the NCS space group *Pna*2$_1$. As shown in Fig. 4, the FBU of CsB$_4$O$_6$F consists of [B$_3$O$_6$] and [BO$_3$F] units. These FBUs further connect together and construct the 2D [B$_4$O$_6$F]$_\infty$ layers of CsB$_4$O$_6$F. Optical measurements reveal that CsB$_4$O$_6$F exhibits a short cutoff edge (155 nm), a large SHG response (1.9 × KDP), and a suitable birefringence (0.127 at 400 nm) that enable frequency doubling down to 171.6 nm. The calculated SHG coefficient (d_{33} = 0.92 pm V^{-1}) and birefringence (0.114 at 1064 nm) agree well with the experimental results. In addition, CsB$_4$O$_6$F possesses a more compact structure compared with KBBF, enabling the facile growth of large single crystals with a better growth habit.

β-BaB$_2$O$_4$ (BBO) is a classic NLO crystal and has been widely used for laser frequency conversion.[43] BBO crystallizes in the NCS space group *R3c* and its structure is shown in Fig. 5, which consists of isolated [B$_3$O$_6$] units and Ba cations. BBO possesses a large SHG coefficient of 1.6 pm V^{-1} (d_{22}) and a large birefringence of 0.125 (at 404 nm) with a UV cutoff edge at 185 nm (corresponding to the bandgap of 6.72 eV). All these
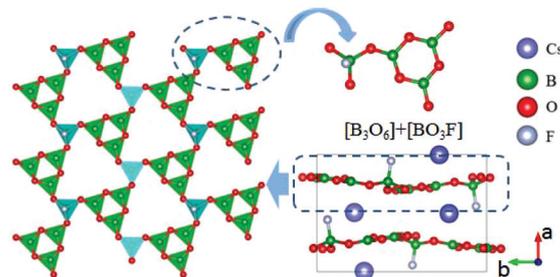

Fig. 4 Crystal structural features of CsB$_4$O$_6$F, whose FBU is composed of [B$_3$O$_6$] and [BO$_3$F].

Fig. 3 Crystal structural features of NH$_4$B$_4$O$_6$F, whose FBU is composed of [BO$_3$] and [BO$_3$F].

Fig. 5 The crystal structure of β-BaB$_2$O$_4$.

This journal is © the Partner Organisations 2020

Inorg. Chem. Front., 2020, **7**, 839–852 | **841**
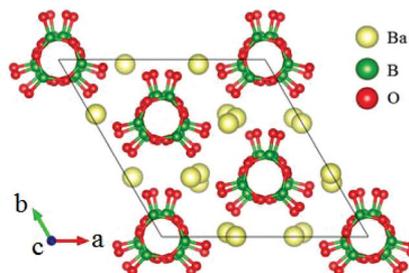
excellent properties guarantee its practical applications as a UV NLO crystal.

2.2 DUV transparent carbonate with planar [CO₃] units

$KSrCO_3F$ belongs to the $ABCO_3F$ (A = K, Rb, Cs; B = Mg, Ca, Sr, Ba) series NLO fluoride carbonates and crystallizes in the NCS space group $P\bar{6}m2$.[44–46] As shown in Fig. 6, its FBU consists of one $[SrO_6F_2]$ polyhedron and three $[CO_3]$ units, which are connected together to form the 2D $[SrCO_3]_\infty$ layer in the $a–b$ plane as shown in Fig. 6b. These layers further construct the 3D framework of $KSrCO_3F$ by sharing the bridging F atoms with K atoms inserted in the space to balance the charges. Large, centimetre-sized single crystals of $KSrCO_3F$ have been grown by top seeded solution growth methods.[47] Based on the obtained crystals, the main optical properties are determined. As per measurements, the UV absorption edge, birefringence and SHG coefficient are 195 nm (corresponding to the bandgap of 6.38 eV), 0.1117 (at 532 nm), and 0.50 pm V^{-1} (d_{22}), respectively. Moreover, $KSrCO_3F$ possesses a large laser damage threshold (LDT) over 700 MW cm^{-2} under a 6 ns Nd:YAG laser operating at 15 Hz. All these properties indicate that $KSrCO_3F$ is an excellent UV NLO material.

$Ca_2Na_3(CO_3)_3F$ crystallizes in the NCS space group Cm and its structure is shown in Fig. 7.[48] Interestingly, the structure of $Ca_2Na_3(CO_3)_3F$ can be described by the substitution of NLO-active $[BO_3]$ units for $[CO_3]$ units from $YCa_4O(BO_3)_3$, which resulted in an optimal balance among the SHG coefficient, birefringence and UV transparency. As per measurements, $Ca_2Na_3(CO_3)_3F$ has a large SHG response of 3 × KDP and a birefringence of 0.082 with the UV absorption edge located at 190 nm (corresponding to the bandgap of 6.53 eV). The calculated largest SHG coefficient and birefringence are about 0.5 pm V^{-1} (d_{12}) and 0.072, respectively, which are in good agreement with the experimental results.

2.3 DUV transparent nitrates with planar [NO₃] units

$Ba_2(OH)_3NO_3$ possesses a hexagonal NCS space group $P\bar{6}2m$ and its structure is shown in Fig. 8.[49] In this compound, the Ba atoms are 9-fold coordinated with O atoms to form a
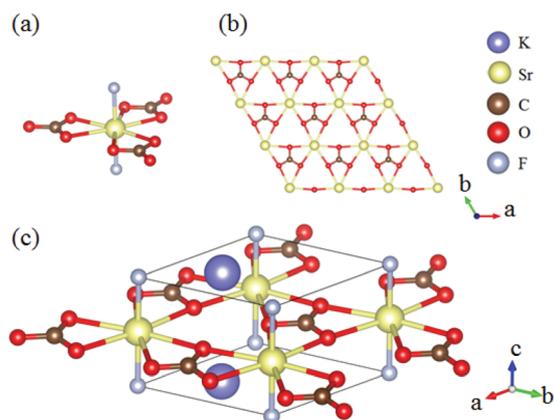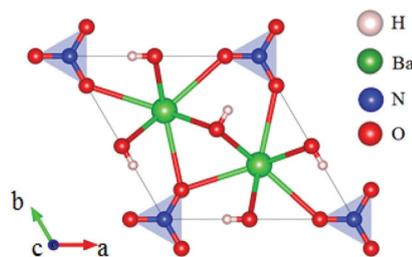

Fig. 7 Crystallographic structure of $Ca_2Na_3(CO_3)_3F$.

Fig. 8 The crystal structure of $Ba_2(OH)_3NO_3$.

$[BaO_3(OH)_6]$ polyhedron, which is further connected with three $[NO_3]$ units to construct the 3D framework of $Ba_2(OH)_3NO_3$. The optical measurements show that $Ba_2(OH)_3NO_3$ has a large SHG response (about 4 times that of KDP) and a birefringence of 0.080 with the UV absorption edge shorter than 200 nm (corresponding to a bandgap of 6.22 eV). Theoretical calculations reveal that the SHG coefficient and birefringence of $Ba_2(OH)_3NO_3$ are 2.41 pm V^{-1} and 0.082, respectively. More importantly, $Ba_2(OH)_3NO_3$ exhibits good water-resistance, making this compound a promising UV NLO material.

Clearly, NLO borates, carbonates, and nitrates can show DUV transparency. For borates, the UV cutoff edges are about 180 nm, and those can be blue-shifted to 150 nm for fluoroox-oborates. For carbonates, F ions must be introduced to achieve deep UV transmission. For nitrates, only two compounds, $i.e.$ $Ba_2(OH)_3NO_3$ and $Sr_2(OH)_3NO_3$, are DUV transparent, while their UV cutoff edges are close to 200 nm. Currently, only borates can achieve the frequency conversion of DUV lasers, while carbonates and nitrates need to further reduce their phase matching wavelengths.

3. UV transparent NLO crystals containing planar π-conjugated groups

Besides the oxygen containing planar π-conjugated groups ($[BO_3]$, $[B_3O_6]$, $[CO_3]$, $[NO_3]$, $[H_xC_3N_3O_3]$), $[BS_3]$ and $[B_3S_6]$ can

Fig. 6 (a) The FBU, (b) $[SrCO_3]$ layer, and (c) the crystal structure of $KSrCO_3F$.

also exhibit transparency in the UV region. Meanwhile, the introduction of distorted polyhedra centered by SALP cations, rare-earth cation centered polyhedra, and metal element centered $[MQ_4]$ tetrahedra will affect their property of transparency. In this section, the related NLO crystals will be discussed.

3.1 UV transparent cyanurates with planar $[H_xC_3N_3O_3]$ groups

LiCl($H_3C_3N_3O_3$) crystallizes in the polar NCS space group $R3m$, as shown in Fig. 9.[50,51] The structure is characterized by graphite-like quasi-2D infinite layers composed of $[H_3C_3N_3O_3]$ units connected by a $[LiO_3Cl]$ tetrahedron (Fig. 9b and c). Interestingly, all the $[H_3C_3N_3O_3]$ units are coplanar and parallel to one another, which is favorable for large SHG response. As per theoretical calculations, LiCl($H_3C_3N_3O_3$) possesses a large SHG coefficient (d_{22} = 4.15 pm V^{-1}) and strong optical anisotropy (Δn = 0.28 at 1064 nm) with a short UV transparent edge of 215 nm, thus showing an attractive prospect for future NLO applications in the solar-blind regions.

β-$Sr_3(C_3N_3O_3)_2$ crystallizes in the NCS space group $R3c$. Its crystal structure is shown in Fig. 10.[28,52] β-$Sr_3(C_3N_3O_3)_2$ is isostructural to the famous NLO crystal BBO, in which the $[B_3O_6]$ is replaced by $[C_3N_3O_3]$. As per measurements, β-$Sr_3(C_3N_3O_3)_2$

has a larger powder SHG response than BBO. To provide a more detailed analysis, first-principles calculations were carried out and the results revealed that the compound has a large SHG coefficient (d_{22} = 3.93 pm V^{-1}) and birefringence (0.36 at 1064 nm) with a UV cutoff edge of about 223 nm. All these optical properties clearly indicated that β-$Sr_3(C_3N_3O_3)_2$ can serve as a UV NLO crystal.

KLi($HC_3N_3O_3$)·$2H_2O$ crystallizes in the NCS space group $Pna2_1$ and its structure is shown in Fig. 11.[53] In this compound, the hydro-isocyanurate $[HC_3N_3O_3]$ units connect with each other through $[LiO_4]$ to form a 1D chain, which further bridges via $[HC_3N_3O_3]$ units to construct an intricate 2D layer as shown in Fig. 11b. As per the determination of optical properties, KLi($HC_3N_3O_3$)·$2H_2O$ shows a large SHG response about 5.3 times that of KDP with a UV cutoff edge of 237 nm (corresponding to the bandgap of 5.23 eV). More importantly, a bulk single crystal with 10 mm × 15 mm × 6 mm in size was obtained. Based on the characterization of the single crystals, KLi($HC_3N_3O_3$)·$2H_2O$ exhibits a high LDT of 4.76 GW cm^{-2} and a large birefringence of 0.186 at 514 nm, which lead to the shortest phase-matching edge to 246 nm.

3.2 UV transparent borates with planar $[BO_3]$ units

$RbZn_2BO_3Br_2$ belongs to the $AZn_2BO_3X_2$ (A = K, Rb, NH$_4$; X = Cl, Br) series NLO materials and only $RbZn_2BO_3Br_2$ is discussed here.[54] The framework of $RbZn_2BO_3Br_2$ can be described by the tetrahedron substitution of $[BeO_3F]$ for $[ZnO_3Br]$ from KBBF as shown in Fig. 12. Optical measurements on $RbZn_2BO_3Br_2$ show that this compound is phase-matchable with powder SHG response about 2.53 times that of KDP and its UV cutoff edge is located at 214 nm, corresponding to the bandgap of 5.79 eV. The first-principles calculations show that its largest SHG coefficient is 0.43 (d_{11}) and reveal that the enhanced SHG response originates from the cooperative effect of coparallel $[BO_3]$ triangles and the distorted $[ZnO_3Br]$ tetrahedron. Moreover, this series of compounds exhibit a lighter layered growth habit than KBBF, which is beneficial for the research of crystal growth.

Pb_2BO_3Cl crystallizes in the trigonal polar NCS space group $P321$ and exhibits a 2D layered structure as shown in Fig. 13.[55]
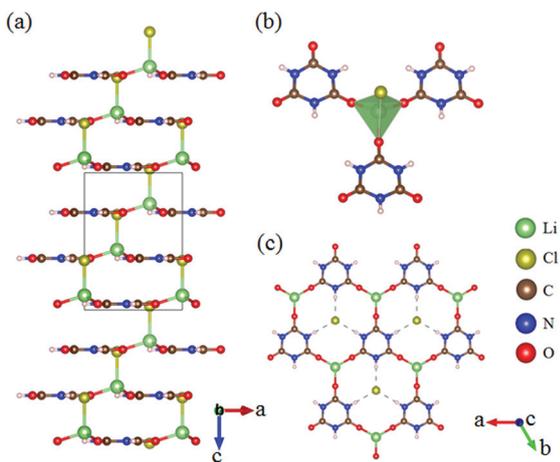

Fig. 9 (a) The crystal structure, (b) FBU, and the $[LiH_3C_3N_3O_3]$ layer of LiCl($H_3C_3N_3O_3$).
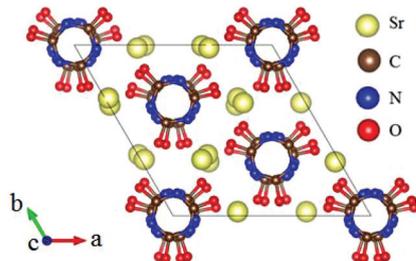

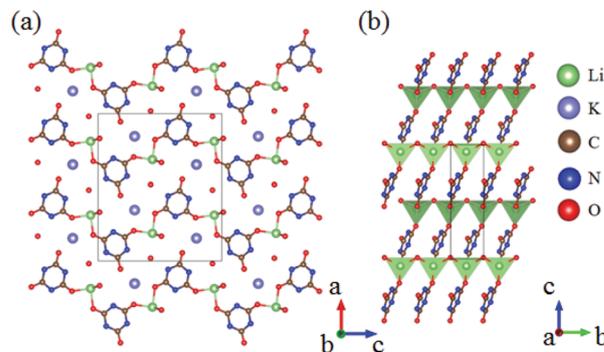**Fig. 10** The crystal structure of β-$Sr_3(C_3N_3O_3)_2$.

Fig. 11 (a) Crystal structure of KLi($HC_3N_3O_3$)·$2H_2O$; (b) layers of KLi($HC_3N_3O_3$)·$2H_2O$ consisting of ($HC_3N_3O_3$) triangular units.

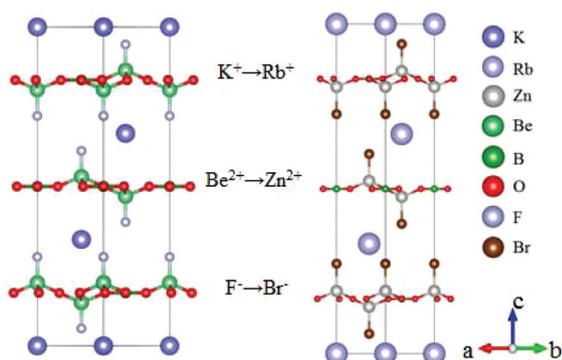This journal is © the Partner Organisations 2020

Inorg. Chem. Front., 2020, **7**, 839–852 | **843**

Fig. 12 Structural evolution from KBBF to $RbZn_2BO_3Br_2$.

Fig. 14 Crystal structure of $Cd_4Y(BO_3)_3$.

Fig. 13 (a) The crystal structure and (b) the $[PbBO_3]$ layer of Pb_2BO_3Cl.
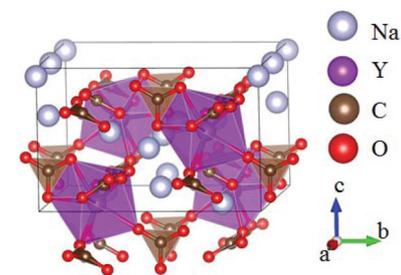
Fig. 15 The crystal structure of $Na_3Y(CO_3)_3$.

Pb_2BO_3Br and Pb_2BO_3I are isomorphic to this compound, which are not discussed here.[56,57] As shown in Fig. 13b, the $[BO_3]$ units are parallelly arranged and connected with a neighbouring $[PbO_3]$ pyramid to construct the 2D infinite $[PbBO_3]$ layers in the a–b plane. Owing to the NLO favourable arrangement of $[BO_3]$, Pb_2BO_3Cl exhibits a large SHG response 9 times that of KDP. It also has a wide transparent window from the UV to mid-IR region with a bandgap of about 3.99 eV. The calculated largest SHG coefficient is about 7.2 pm V^{-1} (d_{11}), which is larger than the experimental result. Its calculated birefringence is 0.12 at 1064 nm, which is in good agreement with the measured phase-matchability.

$Cd_4Y(BO_3)_3$ belongs to the $Cd_4Re(BO_3)_3$ (Re = Y, Gd, Lu) series NLO crystals and crystallizes in the monoclinic NCS space group Cm.[58] There are three kinds of units ($[BO_3]$, $[YO_6]$, and $[CdO_6]$) in this compound as shown in Fig. 14. In $Cd_4Y(BO_3)_3$, these three kinds of units connect together by sharing corners and edges and construct the 3D framework. As per measurements, $Cd_4Y(BO_3)_3$ has a moderate bandgap of 3.78 eV and a large SHG response 5.2 times that of KDP. $Cd_4Y(BO_3)_3$ is also phase-matchable and has wide transparent regions ranging from UV to IR. The first-principles calculations also guaranteed the large SHG response of $Cd_4Y(BO_3)_3$ (the calculated d_{12} = 4.99 pm V^{-1}).

3.3 UV transparent carbonate with planar $[CO_3]$ units

$Na_3Y(CO_3)_3$ crystallizes in the NCS space group $Ama2$ and its structure is shown in Fig. 15.[59] Its crystal structure can be described as alternate stackings of $[Na(CO_3)_2]_\infty$ and $[Na_2Y$
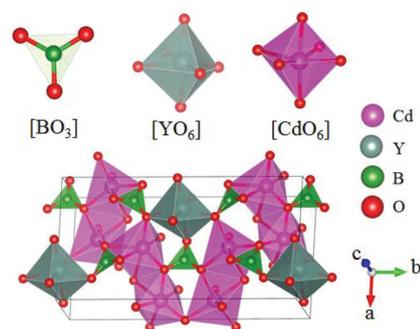
$(CO_3)_2]_\infty$ layers parallel to the b–c plane. SHG measurements show that $Na_3Y(CO_3)_3$ has a large SHG response about 3.57 times that of KDP. It also exhibits wide transparent regions from UV to near IR with short UV cut-off edges at about 220 nm, corresponding to the bandgap of 5.59 eV. Theoretical calculation reveals that its largest SHG coefficient is 1.10 pm V^{-1} (d_{32}). All the mentioned properties suggest that $Na_3Y(CO_3)_3$ is a promising UV NLO crystal.

$CsPbCO_3F$ is isostructural to the aforementioned $KSrCO_3F$. $CsPbCO_3F$ crystallizes in the NCS space group $P\bar{6}m2$ and its structure is shown in Fig. 16.[60] As per measurements, $CsPbCO_3F$ exhibits a smaller bandgap of 4.15 eV but a larger SHG response about 13.4 times that of KDP compared with $KSrCO_3F$. The calculated SHG coefficient is about 5.1 pm V^{-1} (d_{22}), which agrees well with the experimental result. As per the calculated results, it is the p–π interaction between Pb and $[CO_3]$ that resulted in the extremely large SHG efficiency.
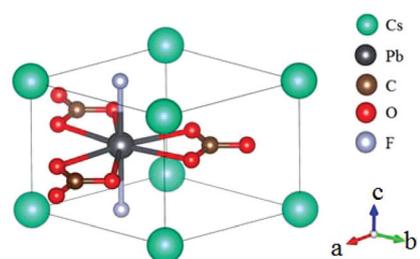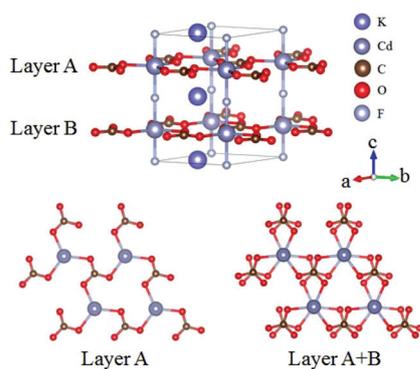

Fig. 16 Crystallographic structure of $CsPbCO_3F$.

844 | *Inorg. Chem. Front.*, 2020, **7**, 839–852

This journal is © the Partner Organisations 2020

Fig. 17 The crystal structure of $KCdCO_3F$, in which the $[CO_3]$ units in neighbouring $[CdCO_3]$ layers exhibit a small rotation.

Fig. 19 The crystal structure of $Bi_3TeO_6OH(NO_3)_2$.

$KCdCO_3F$ belongs to the $ATCO_3F$ (A = K, Rb; T = Zn, Cd) series NLO crystals and here only $KCdCO_3F$ is discussed.[61] $KCdCO_3F$ crystallizes in the NCS space group $P\bar{6}c2$ and its structure is shown in Fig. 17. In $KCdCO_3F$, Cd is 5-fold co-ordinated with 3 O atoms and 2 F atoms and C atoms connect with O atoms to form $[CO_3]$ units. One $[CdO_3F_2]$ connect with three $[CO_3]$ units and construct 2D layers, which are further linked by the bridging-F atoms to form the 3D framework of $KCdCO_3F$. Interestingly, the $[CO_3]$ units in a certain layer are parallelly arranged but exhibit a rotation in two neighbouring layers. As per measurements, $KCdCO_3F$ possesses a large bandgap of 5.30 eV and a SHG response 4.58 times that of KDP. As per calculations, the SHG coefficient and birefrin-gence are 1.99 pm V^{-1} (d_{22}) and 0.11 at 1064 nm, respectively. The $ATCO_3F$ series NLO fluoride carbonates enrich the struc-tural diversity of NLO carbonates and show great potential as UV NLO materials.

3.4 UV transparent nitrates with planar $[NO_3]$ units

$Rb_2Na(NO_3)_3$ crystallizes in the orthorhombic polar NCS space group $Pmc2_1$, as shown in Fig. 18.[62] In this compound, the Na atom is coordinated with 10 oxygen atoms, which are further connected with five $[NO_3]$ units to construct the FBUs. These

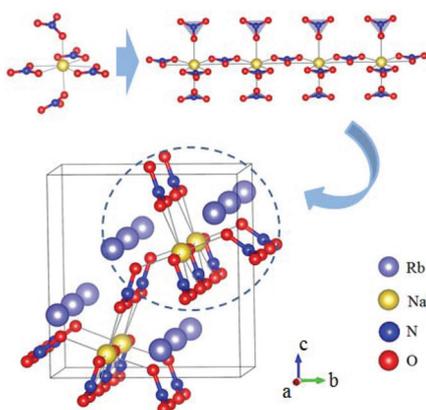FBUs connect together to form a 1D chain with the Rb atoms located between the chains. $Rb_2Na(NO_3)_3$ possesses a large bandgap of about 4.74 eV and exhibits a large SHG response 5 times that of KDP. The calculated largest SHG coefficient (d_{31}) is about 3.48 pm V^{-1}, which agrees well with the experimental result.

$Bi_3TeO_6OH(NO_3)_2$ crystallizes in the NCS monoclinic space group $P2_1$ and its structure contains three kinds of NLO-active units, i.e. planar $[NO_3]$ units, distorted $[TeO_6]$ octahedron, and $[Bi_3O_6H]$ groups with stereochemically active lone pair elec-trons, as shown in Fig. 19.[63] In $Bi_3TeO_6OH(NO_3)_2$, the $[TeO_6]$ octahedron and $[Bi_3O_6H]$ groups connect together to construct the 2D layers extended in the a–b plane with the $[NO_3]$ inserted between the layers. Due to the synergistic effects of these NLO-active units, $Bi_3TeO_6OH(NO_3)_2$ achieved a large SHG response about 3 times that of KDP. The measured bandgap of $Bi_3TeO_6OH(NO_3)_2$ is 3.59 eV, corresponding to the UV cutoff edge of 345 nm. Theoretical calculations reveal that the SHG coefficient and birefringence are d_{16} = −1.31 pm V^{-1} and 0.115 at 1064 nm, respectively. Interestingly, $Bi_3TeO_6OH(NO_3)_2$ is resistant to water, which provided an effective approach for practical nitrate NLO materials with high water-resistance.

3.5 UV transparent sulfides with planar $[BS_3]$ units

BaB_2S_4 crystallizes in the polar space group Cc and its struc-ture is shown in Fig. 20.[64] In BaB_2S_4, the planar $[BS_3]$ units

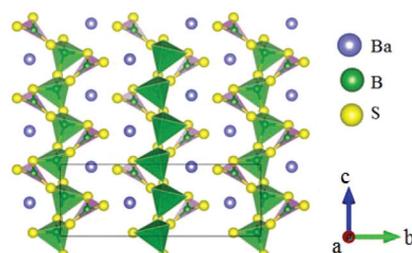**Fig. 18** Crystallographic structure of $Rb_2Na(NO_3)_3$.

Fig. 20 The crystal structure of BaB_2S_4.

This journal is © the Partner Organisations 2020
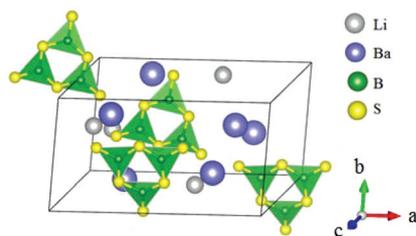
Inorg. Chem. Front., 2020, **7**, 839–852 | **845**

Fig. 21 Crystallographic structure of LiBaB$_3$S$_6$.

and [BS$_4$] tetrahedron are connected with each other by sharing corners to construct 1D infinite zigzag $\frac{1}{\infty}$[B$_2$S$_4$] chains along the c-axis with 8-fold coordinated Ba cations located in the inter-chain. As per measurements, BaB$_2$S$_4$ exhibits a large bandgap of about 3.55 eV, due to which it can achieve a high LDT value during IR NLO applications, which can be preliminarily proven by powder LDT measurement (265 MW cm^{-2}, 1064 nm, 10 ns, 10HZ). The powder SHG measurements show that the compound has a large SHG response about 0.7 times that of AgGaS$_2$ with phase-matchability. The calculated largest SHG coefficient and birefringence are d_{12} = 8.22 pm V^{-1} and 0.11 at 2090 nm, respectively, which agree well with the experimental values. Moreover, BaB$_2$S$_4$ exhibits good air-stability, indicating its potential to become an IR NLO material.

LiBaB$_3$S$_6$ crystallizes in the NCS monoclinic space group Cc and its structure is shown in Fig. 21.[20] As is shown, LiBaB$_3$S$_6$ contains [B$_3$S$_6$] anions formed by three corner-sharing [BS$_3$] units with a six-membered [B$_3$S$_3$] ring inside. The metal cations are located between the anion units with Ba and Li 9- and 4-fold coordinated with sulfur atoms. Theoretical calculations demonstrate that LiBaB$_3$S$_6$ possesses a large bandgap (3.92 eV), thus indicating a high LDT value for mid-IR NLO applications. The birefringence is 0.343 at 1064 nm, which is favorable for achieving phase-matchability. However, the calculated SHG coefficients are rather small (d_{12} = 3.46 pm V^{-1}) owing to the approximately centrosymmetric arrangement of [B$_3$S$_6$] units.

As discussed above, the UV cutoff edges of NLO cyanurates are located at about 230 nm, indicating their applications in the solar-blind regions. The introduction of a polyhedron with SOJT and SALP cations will result in the red shift of the cutoff edges for borates, carbonates and nitrates. In addition, alkalis and alkaline-earth metals containing NLO sulphides with [BS$_3$] and [B$_3$S$_6$] groups possess large bandgaps above 3.3 eV, which would lead to a large LDT for IR NLO applications.

4. VIS transparent NLO crystals containing planar π−conjugated groups

Ba$_3$(BS$_3$)(SbS$_3$) crystallizes in the NCS space group $P\bar{6}2m$ and possesses a 0D structure constructed by isolated trigonal

planar [BS$_3$] units and discrete [SbS$_3$] pyramids, as shown in Fig. 22.[65] Based on the experimental measurements, Ba$_3$(BS$_3$)(SbS$_3$) possesses a moderate bandgap of about 2.62 eV and is transparent in the range of 2.5–11 μm. The SHG response of Ba$_3$(BS$_3$)(SbS$_3$) is three times as large as AgGaS$_2$. The calculated largest NLO coefficient d_{21} is about 2.73 pm V^{-1} and the calculated birefringence is 0.05, which agree well with the powder SHG measurement.

A$_3$VO(O$_2$)$_2$CO$_3$ (A = K, Rb, Cs) is a new series of NLO carbonates. These three compounds are isostructural and crystallize in the NCS space group Cm.[66–68] The structures are composed of distorted [VO(O$_2$)$_2$CO$_3$] FBUs and charge balancing A$^+$ cations as shown in Fig. 23. The measured bandgaps are 2.63 eV, 2.73 eV and 2.81 eV for the K-, Rb-, and Cs-containing compounds, respectively. Their powder SHG effects are 21, 20, and 23 times that of KDP, respectively. It should be noted that Cs$_2$VO(O$_2$)$_2$CO$_3$ showed the largest SHG response among the reported NLO carbonates. The calculated NLO coefficients and birefringence are listed in Table 1. As the theoretical calculations revealed, the [O$_2$] anion groups and [CO$_3$] in [VO(O$_2$)$_2$CO$_3$] FBUs have made huge contributions to the NLO effects.

Bi$_3$TeBO$_9$ crystallizes in the polar hexagonal space group $P6_3$ and its structure is shown in Fig. 24.[69] This compound contains three kinds of NLO-active units, $i.e.$ planar [BO$_3$] units, a SOJT distorted [TeO$_6$] octahedron, and a [BiO$_6$] octahedron with stereochemically active lone pair electrons. These units connect with each other by sharing corners and edges to construct the 3D framework of Bi$_3$TeBO$_9$. Due to the synergistic effects of these units, Bi$_3$TeBO$_9$ has achieved the largest SHG responses 20 times that of KDP among the ever-reported borate NLO crystals. The bandgap of this compound is found to be 3.23 eV, which is located in the VIS region. In addition, theoretical calculations show that this compound has a larger NLO coefficient d_{33} of about 5.1 pm V^{-1} and reveal that such a large SHG response resulted from the synergistic effects of constituted NLO-active groups.

By introducing more than one bandgap-reducing units ([O$_2$], [VO$_x$] polyhedron, [TeO$_6$] and [BiO$_6$]), the UV transparent edges of borates and carbonates can be red shifted to the VIS region. Meanwhile, owing to the synergistic effects of multiple NLO-active units, the largest SHG responses of both NLO borates and carbonates are achieved, which will promote the exploration of materials with high laser frequency conversion efficiency in the visible spectrum region.
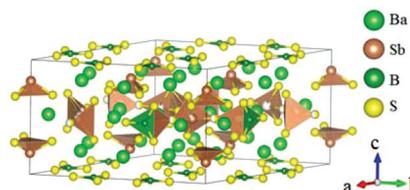

Fig. 22 Crystallographic structure of Ba$_3$(BS$_3$)(SbS$_3$).

846 | *Inorg. Chem. Front.*, 2020, **7**, 839–852

This journal is © the Partner Organisations 2020

Table 1 The main optical properties of the compounds containing the inorganic planar NLO-active groups

Compounds	Space group	Planar units	Bandgap (eV)	Exp. SHG response	Largest SHG coefficient (pm V^{-1})	Birefringence	Ref.
DUV (E_g > 6.22 eV)							
γ-Be$_2$BO$_3$F	$R32$	[BO$_3$]	8.56[a]	2.3 × KDP	d_{11} = 0.67[a]	0.105(@400 nm)[a]	37
KBe$_2$BO$_3$F$_2$	$R32$	[BO$_3$]	8.46	1.3 × KDP	d_{11} = 0.47	0.088(@400 nm)	5,12
NH$_4$Be$_2$BO$_3$F$_2$	$R32$	[BO$_3$]	8.10	1.2 × KDP	d_{11} = 0.43	0.078(@400 nm)	37
CsB$_4$O$_6$F	$Pna2_1$	[B$_3$O$_6$]	8.03	1.9 × KDP	d_{33} = 0.92[a]	0.127(@400 nm)	40
NH$_4$B$_4$O$_6$F	$Pna2_1$	[BO$_3$]	7.97	2.5 × KDP	d_{33} = −1.19[a]	0.130(@407 nm)	39
BaB$_2$O$_4$	$R3c$	[B$_3$O$_6$]	6.72	5.6 × KDP	d_{22} = 1.60	0.125(@404 nm)	43
Li$_4$Sr(BO$_3$)$_2$	Cc	[BO$_3$]	6.69	2 × KDP	d_{12} = 0.64[a]	0.056(@532 nm)[a]	38
Ca$_2$Na$_3$(CO$_3$)$_3$F	Cc	[CO$_3$]	6.53	3 × KDP	d_{33} = 0.5[a]	0.082(@589.6 nm)	48
KSrCO$_3$F	$P\bar{6}m2$	[CO$_3$]	6.38	3.33 × KDP	d_{22} = 0.50	0.112(@532 nm)	44,47
Ba$_2$(OH)$_3$NO$_3$	$P\bar{6}2m$	[NO$_3$]	>6.22	4 × KDP	d_{22} = 2.41[a]	0.080(@532 nm)	49
UV (3.27 eV < E_g < 6.22 eV)							
RbZn$_2$BO$_3$Br$_2$	$R32$	[BO$_3$]	5.79	2.53 × KDP	d_{11} = 0.43[a]	—	54
LiCl(H$_3$C$_3$N$_3$O$_3$)	$R3m$	[H$_3$C$_3$N$_3$O$_3$]	5.76[a]	—	d_{22} = 4.15[a]	0.28(@800 nm)[a]	50
Na$_3$Y(CO$_3$)	$Ama2$	[CO$_3$]	5.59	3.57 × KDP	d_{32} = 1.10[a]	—	59
β-Sr$_3$(C$_3$N$_3$O$_3$)$_2$	$R3c$	[C$_3$N$_3$O$_3$]	5.57[a]	>BBO	d_{22} = 3.93[a]	0.36(@1064 nm)[a]	28,52
KCdCO$_3$F	$P\bar{6}c2$	[CO$_3$]	5.30	4.58 × KDP	d_{22} = 1.99[a]	0.11(@1064 nm)[a]	61
KLi(HC$_3$N$_3$O$_3$)·2H$_2$O	$Pna2_1$	[HC$_3$N$_3$O$_3$]	5.23	5.3 × KDP	d_{33} > 1.95	0.186(@514 nm)	53
Rb$_2$Na(NO$_3$)$_3$	$Pmc2_1$	[NO$_3$]	4.74	5 × KDP	d_{31} = 3.48	—	62
CsPbCO$_3$F	$P\bar{6}m2$	[CO$_3$]	4.15	13.4 × KDP	d_{22} = 5.1[a]	—	60
Pb$_2$BO$_3$Cl	$P321$	[BO$_3$]	3.99	9 × KDP	d_{11} = 7.2[a]	0.12(@1064 nm)[a]	55
LiBaB$_3$S$_6$	Cc	[B$_3$S$_6$]	3.92[a]	—	d_{12} = 3.46[a]	0.343(@1064 nm)[a]	20
Cd$_4$YO(BO$_3$)$_3$	Cm	[BO$_3$]	3.78	5.2 × KDP	d_{12} = 4.99[a]	—	58
Bi$_3$TeO$_6$OH(NO$_3$)$_2$	$P21$	[NO$_3$]	3.59	3 × KDP	d_{16} = −1.31[a]	0.115(@1064 nm)[a]	63
BaB$_2$S$_4$	Cc	[BS$_3$]	3.55	0.7 × AGS	d_{12} = 8.22[a]	0.11(@2090 nm)[a]	64
VIS (1.59 eV < E_g < 3.27 eV)							
Bi$_3$TeBO$_9$	$P6_3$	[BO$_3$]	3.23	20 × KDP	d_{33} = 5.1[a]	—	69
Cs$_3$VO(O$_2$)$_2$CO$_3$	Cm	[CO$_3$]	2.81	23 × KDP	d_{13} = 8.7[a]	0.105(@1064 nm)[a]	68
Rb$_3$VO(O$_2$)$_2$CO$_3$	Cm	[CO$_3$]	2.73	20 × KDP	d_{24} = 7.5	0.075(@1064 nm)[a]	67
K$_3$VO(O$_2$)$_2$CO$_3$	Cm	[CO$_3$]	2.63	21 × KDP	d_{11} = 8.21	—	66
Ba$_3$(BS$_3$)(SbS$_3$)	$P\bar{6}2m$	[BS$_3$]	2.62	3 × AGS	d_{21} = 2.73	0.050(static)	65
IR (E_g < 1.59 eV)							
BaHgSe$_2$	$Pmc2_1$	[HgSe$_3$]	1.56	1.5 × AGS	d_{33} = 39.87[a]	0.147(@2090 nm)[a]	70
Na$_2$BP$_2$	$Pmc2_1$	[B$_2$P$_5$]	1.10	—	d_{12} = 57.14[a]	0.68(@2090 nm)[a]	73
Ag$_6$HgSiSe$_6$	$Pmn2_1$	[AgSe$_3$]	1.00	2 × AGS	d_{32} = 43.22[a]	0.233(@2090 nm)[a]	71
Ag$_6$HgGeSe$_6$	$Pmn2_1$	[AgSe$_3$]	0.92	0.5 × AGS	d_{32} = 21.36[a]	0.207(@2090 nm)[a]	71

[a] Calculated results by DFT methods.
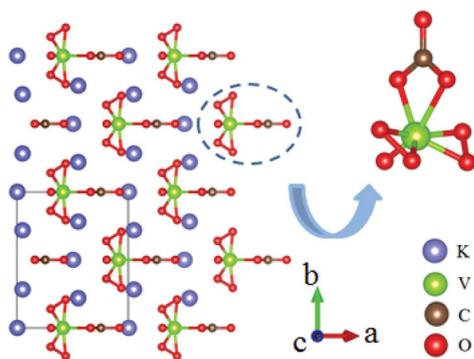
Fig. 23 The crystal structure of A$_3$VO(O$_2$)$_2$CO$_3$.
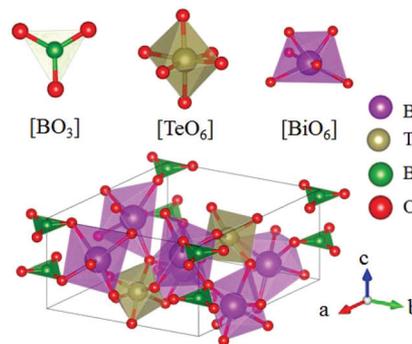
Fig. 24 The crystal structure of Bi$_3$TeBO$_9$.

5. IR transparent NLO crystals containing planar π-conjugated groups

BaHgSe$_2$ belongs to the orthorhombic NCS space group $Pmc2_1$ and its structure is shown in Fig. 25.[70] In its structure, the Hg atoms have two different coordinated environments, where Hg1 atoms are coordinated to three Se atoms to form trigonal planar [HgSe$_3$] units, while Hg2 atoms are bonded to two Se atoms to construct the [HgSe$_2$] linear units. The [HgSe$_3$] units connect with each other by sharing the bridging Se atoms and construct a 1D infinite chain along the a-axis, which will lead to large SHG responses. As per measure-
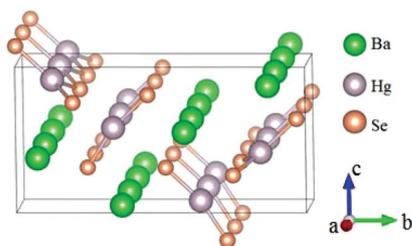
This journal is © the Partner Organisations 2020

Inorg. Chem. Front., 2020, **7**, 839–852 | **847**

Fig. 25 Crystallographic structure of $BaHgSe_2$.

ments, the bandgap of $BaHgSe_2$ is about 1.56 eV and its SHG response is about 1.5 times that of $AgGeS_2$. Moreover, the calculated largest SHG coefficient d_{33} is about 39.87 pm V^{-1} and the birefringence is 0.147 at 2090 nm. $BaHgSe_2$ also exhibits good physicochemical stability, holding great promise for IR NLO applications.

$Ag_6HgSiSe_6$ and $Ag_6HgGeSe_6$ possess similar structures and both of them crystallize in the NCS space group $Pnm2_1$, the FBUs and the structures of which are shown in Fig. 26 and 27, respectively.[71] In $Ag_6HgSiSe_6$, $[Ag/HgSe_3]$ and $[SiSe_4]$ are connected alternately to form 1D $[HgSiSe_5]$ chains along the b-axis, which are further linked with each other's chains *via* $[AgSe_3]$ and $[AgSe_4]$ to construct the 3D framework of $Ag_6HgSiSe_6$. It should be noted that the planar $[Ag/HgSe_3]$ units are aligned completely parallel to each other in the 1D
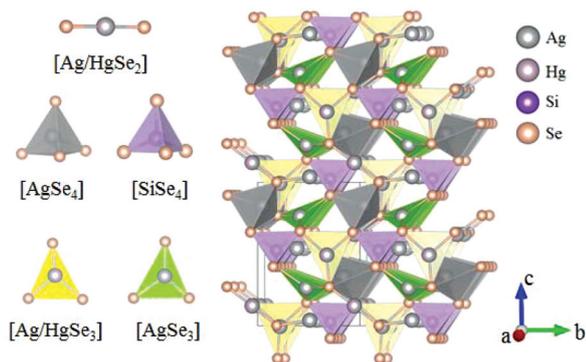

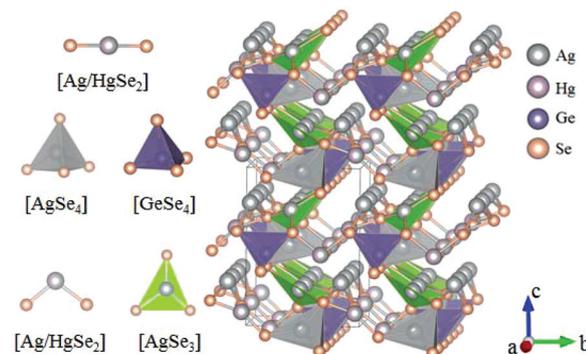**Fig. 26** Crystallographic structure of $Ag_6HgSiSe_6$.

Fig. 27 Crystallographic structure of $Ag_6HgGeSe_6$.

$[HgSiSe_5]$ chains, which would be the main origin of the large SHG responses of $Ag_6HgSiSe_6$. $Ag_6HgGeSe_6$ adopts a similar structure to that of $Ag_6HgSiSe_6$, but its $[Ag/HgSe_3]$ units degenerate into $[Ag/HgSe_2]$, thus reducing the second-order non-linear polarizability of $Ag_6HgGeSe_6$. As per the measurements, the bandgaps of $Ag_6HgSiSe_6$ and $Ag_6HgGeSe_6$ are 1.00 eV and 0.92 eV, respectively. The measured powder SHG effects of these two compounds are 2 and 0.5 times that of $AgGaS_2$, which agree well with the calculated SHG coefficients ($d_{32} = 43.22$ pm V^{-1} for $Ag_6HgSiSe_6$ and $d_{32} = 21.36$ pm V^{-1} for $Ag_6HgGeSe_6$). The calculated birefringence for $Ag_6HgSiSe_6$ and $Ag_6HgGeSe_6$ is 0.233 and 0.207 at 2090 nm, respectively. In addition, these two compounds are congruent-melting. All the mentioned features (such as strong SHG responses, valuable phase-matchable features, and congruent-melting thermal behaviour) make $Ag_6HgSiSe_6$ and $Ag_6HgGeSe_6$ promising IR NLO crystals for practical applications.

Na_2BP_2 was obtained by oxidative elimination reactions and it crystallizes in the $Pmc2_1$ space group (Fig. 28).[72] In this compound, the B atoms are three coordinated with P atoms to construct the planar $[BP_3]$ triangles. Every two $[BP_3]$ units are bonded by a corner-sharing P atom and two bridging P atoms to form a $[B_2P_5]$ 5-membered ring. These unique $[B_2P_5]$ FBUs further connect with each other by sharing the exocyclic P atoms and construct a 1D infinite chain. All these chains are arranged along the a-axis with an inclined angle of $\sim 90°$ in the $b–c$ plane between the adjacent chains. The bandgap of Na_2BP_2 is about 1.10 eV, indicating its shortwave cutoff edge located in the IR regions. Due to the absence of experimental data, the first principles calculations were carried out.[73] As the results revealed, Na_2BP_2 possesses both the largest birefringence ($\Delta n \sim 0.68$) and nonlinearity ($d_{15} \sim 57.14$ pm V^{-1}) among all known inorganic NLO materials containing planar NLO-active groups, which make $[B_2P_5]$ a good NLO-active unit and inspire a new direction for designing high-performance NLO materials.

In this section, IR NLO materials with planar $[HgSe_3]$, $[AgSe_3]$, and $[B_2P_5]$ units are discussed. These crystals possess both huge SHG responses and birefringence, which make these units good candidates to achieve high conversion efficiency for IR NLO applications.
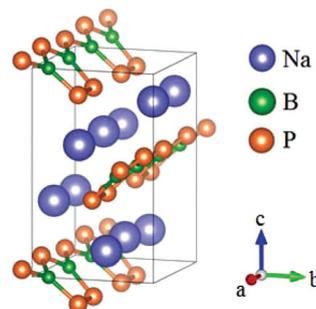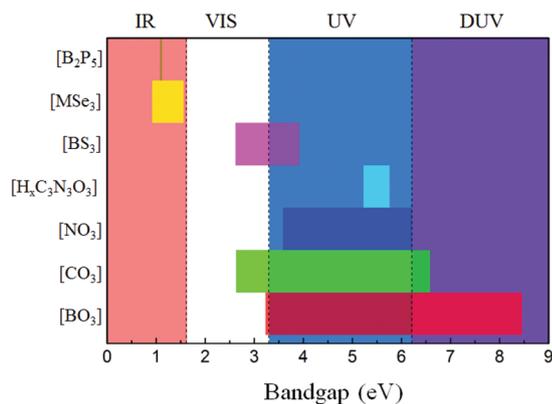

Fig. 28 Crystallographic structure of Na_2BP_2.

Fig. 29 The distribution plot of bandgaps for the involved NLO materials with different planar π-conjugated groups.

6. Conclusions

The main optical properties of the above-mentioned NLO materials containing inorganic planar NLO-active groups are listed in Table 1. All the mentioned NLO crystals exhibit large SHG responses and birefringence, indicating their potential in NLO applications. Specifically, the ordered arrangement of $[BO_3]$ units leads to the SHG response about 1.3 times that of KDP (KBBF), which could be enhanced to about 2 × KDP by modifying its density (AB_4O_6F series), and further enlarged to 20 × KDP (Bi_3TeBO_9) by introducing other NLO-active units. For NLO carbonates, the SHG responses are about 3 × KDP for the orderly arranged $[CO_3]$ units ($KSrCO_3F$), which can further be enlarged to 23 × KDP ($Cs_3VO(O_2)_2CO_3$) by the synergistic effects with other kinds of NLO-active units. The orderly arranged $[NO_3]$ units lead to a response of about 4 × KDP, which is much larger than those of the $[BO_3]$ and $[CO_3]$ units. For the $[H_xC_3N_3O_3]$ units, the SHG responses vary from 5 to 10 times that of KDP, which are dependent on their arrangement and density. For the no-oxygen-containing planar π-conjugated groups, the SHG responses are comparable to or even larger than that of AGS, which is suitable for IR NLO applications. In addition, most of the reported NLO materials containing inorganic planar NLO-active groups are phase-matchable, which indicated sufficient birefringence for practical applications.

To investigate the property of transparency of the planar π-conjugated groups, the distribution plots of the bandgaps of the involved NLO materials are drawn in Fig. 29. As is shown, only the bandgaps of $[BO_3]$ and $[CO_3]$ can cover the regions from VIS to DUV. $[NO_3]$ covers the UV and DUV regions, but its largest bandgap can only touch the DUV region, which makes NLO nitrates not suitable for DUV laser frequency conversion.[27,74] The bandgaps of NLO cyanurates are mainly located at about 5.5 eV, which is beneficial for laser frequency conversion in the solar blind region. NLO materials containing $[BS_3]$ groups possess bandgaps covering the VIS and UV regions, which would lead to a large LDT for IR NLO applications. For the NLO compounds containing $[MSe_3]$ and $[B_2P_5]$ units, the bandgaps are located in the IR region. Therefore, by

summarising the property of transparency, the potential applied wave ranges of various planar π-conjugated groups are evaluated.

In my opinion, inorganic planar NLO-active groups are one of the most desirable FBUs to construct NLO materials. Firstly, they possess large SHG responses and optical anisotropy, which are beneficial for NLO applications. Secondly, their bandgaps cover the whole wave ranges from DUV to IR, indicating that one can find suitable NLO materials with planar NLO-active groups for laser frequency conversion in a certain wave range. However, compared to the oxygen containing planar units, the kinds of no-oxygen containing planar units and the structural diversity of NLO compounds with these units are limited. For further development, NLO materials with new no-oxygen containing planar NLO-active groups should be considered.

Conflicts of interest

There are no conflicts to declare.

Acknowledgements

Notes and references

1 V. Petrov, Frequency down-conversion of solid-state laser sources to the mid-infrared spectral range using non-oxide nonlinear crystals, *Prog. Quantum Electron.*, 2015, **42**, 1–106.

2 M. Pushkarsky, A. Tsekoun, I. G. Dunayevskiy, R. Go and C. K. N. Patel, Sub-parts-per-billion level detection of NO_2 using room-temperature quantum cascade lasers, *Proc. Natl. Acad. Sci. U. S. A.*, 2006, **103**, 10846–10849.

3 N. Savage, Ultraviolet lasers, *Nat. Photonics*, 2007, **1**, 83–85.

4 N. Savage, Photodetectors, *Nat. Photonics*, 2007, **1**, 730–731.

5 C. T. Chen, G. L. Wang, X. Y. Wang and Z. Y. Xu, Deep-UV nonlinear optical crystal $KBe_2BO_3F_2$-discovery, growth, optical properties and applications, *Appl. Phys. B: Lasers Opt.*, 2009, **97**, 9–25.

6 D. Cyranoski, Materials science: China's crystal cache, *Nature*, 2009, **457**, 953–955.

7 Y. Zhou, G.-L. Wang, C.-M. Li, Q.-J. Peng, D.-F. Cui, Z.-Y. Xu, X.-Y. Wang, Y. Zhu, C.-T. Chen, G.-D. Liu, X.-L. Dong and X.-J. Zhou, Sixth harmonic of a Nd : YVO$_4$ laser generation in KBBF for ARPES, *Chin. Phys. Lett.*, 2008, **25**, 963–965.

8 C. T. Chen, B. C. Wu, A. D. Jiang and G. M. You, A new type ultraviolet SHG crystal: beta-BaB_2O_4, *Sci. Sin., Ser. B*, 1985, **28**, 235–243.

This journal is © the Partner Organisations 2020

Inorg. Chem. Front., 2020, **7**, 839–852 | **849**

9 C. T. Chen, Y. C. Wu, A. D. Jiang, B. C. Wu, G. M. You, R. K. Li and S. J. Lin, New Nonlinear Optical Crystal: LiB_3O_5, *J. Opt. Soc. Am. B*, 1989, **6**, 616–621.

10 J. D. Bierlein and H. Vanherzeele, Potassium Titanyl Phosphat Properties and New Applications, *J. Opt. Soc. Am. B*, 1989, **6**, 622–633.

11 G. D. Boyd, H. Kasper and J. H. McFee, Linear and nonlinear optical properties of $AgGaS_2$, $CuGaS_2$, and $CuInS_2$, and theory of wedge technique for measurement of nonlinear coefficients, *IEEE J. Quantum Electron.*, 1971, **QE 7**, 563–573.

12 C. Chen, T. Sasaki, R. Li, Y. Wu, Z. Lin, Y. Mori, Z. Hu, J. Wang, G. Aka, M. Yoshimura and Y. Kaneda, *Nonlinear Optical Borate Crystals: Principals and Applications*, Wiley-VCH press, Germany, 2012.

13 Z. Lin, X. Jiang, L. Kang, P. Gong, S. Luo and M.-H. Lee, First-principles materials applications and design of nonlinear optical crystals, *J. Phys. D: Appl. Phys.*, 2014, **47**, 253001.

14 P. Gong, F. Liang, L. Kang, X. Chen, J. Qin, Y. Wu and Z. Lin, Recent advances and future perspectives on infrared nonlinear optical metal halides, *Coord. Chem. Rev.*, 2019, **380**, 83–102.

15 L. Kang, M. Zhou, J. Yao, Z. Lin, Y. Wu and C. Chen, Metal Thiophosphates with Good Mid-infrared Nonlinear Optical Performances: A First-Principles Prediction and Analysis, *J. Am. Chem. Soc.*, 2015, **137**, 13049–13059.

16 F. Liang, L. Kang, Z. Lin, Y. Wu and C. Chen, Analysis and prediction of mid-IR nonlinear optical metal sulfides with diamond-like structures, *Coord. Chem. Rev.*, 2017, **333**, 57–70.

17 L. Kang, F. Liang, X. Jiang, Z. Lin and C. Chen, First-Principles Design and Simulations Promote the Development of Nonlinear Optical Crystals, *Acc. Chem. Res.*, 2019, DOI: 10.1021/acs.accounts.9b00448.

18 L. Kang, D. M. Ramo, Z. Lin, P. D. Bristowe, J. Qin and C. Chen, First principles selection and design of mid-IR nonlinear optical halide crystals, *J. Mater. Chem. C*, 2013, **1**, 7363–7370.

19 W. Yao, R. He, X. Wang, Z. Lin and C. Chen, Analysis of Deep-UV Nonlinear Optical Borates: Approaching the End, *Adv. Opt. Mater.*, 2014, **2**, 411–417.

20 F. Liang, L. Kang, Z. Lin and Y. Wu, Mid-Infrared Nonlinear Optical Materials Based on Metal Chalcogenides: Structure-Property Relationship, *Cryst. Growth Des.*, 2017, **17**, 2254–2289.

21 K. M. Ok, P. S. Halasyamani, D. Casanova, M. Llunell, P. Alemany and S. Alvarez, Distortions in octahedrally co-ordinated d^0 transition metal oxides: A continuous symmetry measures approach, *Chem. Mater.*, 2006, **18**, 3176–3183.

22 R. He, Z. S. Lin, M. H. Lee and C. T. Chen, Ab initio studies on the mechanism for linear and nonlinear optical effects in $YAl_3(BO_3)_4$, *J. Appl. Phys.*, 2011, **109**, 103510.

23 R. Cong, Y. Wang, L. Kang, Z. Zhou, Z. Lin and T. Yang, An outstanding second-harmonic generation material BiB_2O_4F: exploiting the electron-withdrawing ability of fluorine, *Inorg. Chem. Front.*, 2015, **2**, 170–176.

24 Y. Shen, S. Zhao and J. Luo, The role of cations in second-order nonlinear optical materials based on pi-conjugated $[BO_3]^{3-}$ groups, *Coord. Chem. Rev.*, 2018, **366**, 1–28.

25 G. Han, Y. Wang, B. Zhang and S. Pan, Fluorooxoborates: Ushering in a New Era of Deep Ultraviolet Nonlinear Optical Materials, *Chem. – Eur. J.*, 2018, **24**, 17638–17650.

26 L. Kang, S. Luo, H. Huang, N. Ye, Z. Lin, J. Qin and C. Chen, Prospects for Fluoride Carbonate Nonlinear Optical Crystals in the UV and Deep-UV Regions, *J. Phys. Chem. C*, 2013, **117**, 25684–25692.

27 X. Liu, P. Gong, Y. Yang, G. Song and Z. Lin, Nitrate nonlinear optical crystals: A survey on structure-performance relationships, *Coord. Chem. Rev.*, 2019, **400**, 213045.

28 F. Liang, L. Kang, X. Zhang, M.-H. Lee, Z. Lin and Y. Wu, Molecular Construction Using $(C_3N_3O_3)^{3-}$ Anions: Analysis and Prospect for Inorganic Metal Cyanurates Nonlinear Optical Materials, *Cryst. Growth Des.*, 2017, **17**, 4015–4020.

29 X. Meng, F. Liang, K. Kang, J. Tang, T. Zeng, Z. Lin and M. Xia, Facile Growth of an Ultraviolet Hydroisocyanurate Crystal with Strong Nonlinearity and a Wide Phase-Matching Region from π-Conjugated $(HC_3N_3O_3)^{2-}$ Groups, *Inorg. Chem.*, 2019, **58**, 11289–11293.

30 X. Meng, F. Liang, J. Tang, K. Kang, Q. Huang, W. Yin, Z. Lin and M. Xia, $Cs_3Na(H_2C_3N_3O_3)_4 \cdot 3H_2O$: A Mixed Alkali-Metal Hydroisocyanurate Nonlinear Optical Material Containing pi-Conjugated Six-Membered-Ring Units, *Eur. J. Inorg. Chem.*, 2019, 2791–2795.

31 M. Xia, M. Zhou, F. Liang, X. Meng, J. Yao, Z. Lin and R. Li, Noncentrosymmetric Cubic Cyanurate $K_6Cd_3(C_3N_3O_3)_4$ Containing Isolated Planar pi-Conjugated $(C_3N_3O_3)^{3-}$ Groups, *Inorg. Chem.*, 2018, **57**, 32–36.

32 J. Lu, Y.-K. Lian, L. Xiong, Q.-R. Wu, M. Zhao, K.-X. Shi, L. Chen and L.-M. Wu, How To Maximize Birefringence and Nonlinearity of π-Conjugated Cyanurates, *J. Am. Chem. Soc.*, 2019, **141**, 16151–16159.

33 M. Mutailipu, M. Zhang, Z. Yang and S. Pan, Targeting the Next Generation of Deep-Ultraviolet Nonlinear Optical Materials: Expanding from Borates to Borate Fluorides to Fluorooxoborates, *Acc. Chem. Res.*, 2019, **52**, 791–801.

34 C. Wu, G. Yang, M. G. Humphrey and C. Zhang, Recent advances in ultraviolet and deep-ultraviolet second-order nonlinear optical crystals, *Coord. Chem. Rev.*, 2018, **375**, 459–488.

35 Y. Pan, S.-P. Guo, B.-W. Liu, H.-G. Xue and G.-C. Guo, Second-order nonlinear optical crystals with mixed anions, *Coord. Chem. Rev.*, 2018, **374**, 464–496.

36 T. T. Tran, H. Yu, J. M. Rondinelli, K. R. Poeppelmeier and P. S. Halasyamani, Deep Ultraviolet Nonlinear Optical Materials, *Chem. Mater.*, 2016, **28**, 5238–5258.

37 G. Peng, N. Ye, Z. Lin, L. Kang, S. Pan, M. Zhang, C. Lin, X. Long, M. Luo, Y. Chen, Y.-H. Tang, F. Xu and T. Yan, $NH_4Be_2BO_3F_2$ and γ-Be_2BO_3F: Overcoming the Layering Habit in $KBe_2BO_3F_2$ for the Next-Generation Deep-Ultraviolet Nonlinear Optical Materials, *Angew. Chem., Int. Ed.*, 2018, **57**, 8968–8972.

38 S. Zhao, P. Gong, L. Bai, X. Xu, S. Zhang, Z. Sun, Z. Lin, M. Hong, C. Chen and J. Luo, Beryllium-free Li$_4$Sr(BO$_3$)$_2$ for deep-ultraviolet nonlinear optical applications, *Nat. Commun.*, 2014, **5**, 4019.

39 G. Shi, Y. Wang, F. Zhan, B. Zhang, Z. Yang, X. Hou, S. Pan and K. R. Poeppelmeier, Finding the Next Deep-Ultraviolet Nonlinear Optical Material: NH$_4$B$_4$O$_6$F, *J. Am. Chem. Soc.*, 2017, **139**, 10645–10648.

40 X. Wang, Y. Wang, B. Zhang, F. Zhang, Z. Yang and S. Pan, CsB$_4$O$_6$F: A Congruent-Melting Deep-Ultraviolet Nonlinear Optical Material by Combining Superior Functional Units, *Angew. Chem., Int. Ed.*, 2017, **56**, 14119–14123.

41 B. Zhang, G. Shi, Z. Yang, F. Zhang and S. Pan, Fluorooxoborates: Beryllium-Free Deep-Ultraviolet Nonlinear Optical Materials without Layered Growth, *Angew. Chem., Int. Ed.*, 2017, **56**, 3916–3919.

42 Z. Zhang, Y. Wang, B. Zhang, Z. Yang and S. Pan, Polar Fluorooxoborate, NaB$_4$O$_6$F: A Promising Material for Ionic Conduction and Nonlinear Optics, *Angew. Chem., Int. Ed*, 2018, **57**, 6577–6581.

43 J. Lin, M. H. Lee, Z. P. Liu, C. T. Chen and C. J. Pickard, Mechanism for linear and nonlinear optical effects in β-BaB$_2$O$_4$ crystals, *Phys. Rev. B: Condens. Matter Mater. Phys.*, 1999, **60**, 13380–13389.

44 G. Zou, N. Ye, L. Huang and X. Lin, Alkaline-Alkaline Earth Fluoride Carbonate Crystals ABCO$_3$F (A = K, Rb, Cs; B = Ca, Sr, Ba) as Nonlinear Optical Materials, *J. Am. Chem. Soc.*, 2011, **133**, 20001–20007.

45 T. T. Tran, J. He, J. M. Rondinelli and P. S. Halasyamani, RbMgCO$_3$F: A New Beryllium-Free Deep-Ultraviolet Nonlinear Optical Material, *J. Am. Chem. Soc.*, 2015, **137**, 10504–10507.

46 T. T. Tran, J. Young, J. M. Rondinelli and P. S. Halasyamani, Mixed-Metal Carbonate Fluorides as Deep-Ultraviolet Nonlinear Optical Materials, *J. Am. Chem. Soc.*, 2017, **139**, 1285–1295.

47 W. Zhang and P. S. Halasyamani, Crystal growth and optical properties of a UV nonlinear optical material KSrCO$_3$F, *CrystEngComm*, 2017, **19**, 4742–4748.

48 M. Luo, Y. Song, C. Lin, N. Ye, W. Cheng and X. Long, Molecular Engineering as an Approach To Design a New Beryllium-Free Fluoride Carbonate as a Deep-Ultraviolet Nonlinear Optical Material, *Chem. Mater.*, 2016, **28**, 2301–2307.

49 X. Dong, L. Huang, Q. Liu, H. Zeng, Z. Lin, D. Xu and G. Zou, Perfect balance harmony in Ba$_2$NO$_3$(OH)$_3$: a beryllium-free nitrate as a UV nonlinear optical material, *Chem. Commun.*, 2018, **54**, 5792–5795.

50 F. Liang, N. Wang, X. Liu, Z. Lin and Y. Wu, Co-crystal LiCl·(H$_3$C$_3$N$_3$O$_3$): a promising solar-blind nonlinear optical crystal with giant nonlinearity from coplanar π-conjugated groups, *Chem. Commun.*, 2019, **55**, 6257–6260.

51 O. Shemchuk, D. Braga, L. Maini and F. Grepioni, Anhydrous ionic co-crystals of cyanuric acid with LiCl and NaCl, *CrystEngComm*, 2017, **19**, 1366–1369.

52 M. Kalmutzki, M. Stroebele, F. Wackenhut, A. J. Meixner and H. J. Meyer, Synthesis and SHG Properties of Two New Cyanurates: Sr$_3$(O$_3$C$_3$N$_3$)$_2$ (SCY) and Eu$_3$(O$_3$C$_3$N$_3$)$_2$ (ECY), *Inorg. Chem.*, 2014, **53**, 12540–12545.

53 D. Lin, M. Luo, C. Lin, F. Xu and N. Ye, KLi (HC$_3$N$_3$O$_3$)·2H$_2$O: Solvent-drop Grinding Method toward the Hydro-isocyanurate Nonlinear Optical Crystal, *J. Am. Chem. Soc.*, 2019, **141**, 3390–3394.

54 G. Yang, P. Gong, Z. Lin and N. Ye, AZn$_2$BO$_3$X$_2$(A = K, Rb, NH4; X = Cl, Br): New Members of KBBF Family Exhibiting Large SHG Response and the Enhancement of Layer Interaction by Modified Structures, *Chem. Mater.*, 2016, **28**, 9122–9131.

55 G. Zou, C. Lin, H. Jo, G. Nam, T.-S. You and K. M. Ok, Pb$_2$BO$_3$Cl: A Tailor-Made Polar Lead Borate Chloride with Very Strong Second Harmonic Generation, *Angew. Chem., Int. Ed.*, 2016, **55**, 12078–12082.

56 M. Luo, Y. Song, F. Liang, N. Ye and Z. Lin, Pb$_2$BO$_3$Br: a novel nonlinear optical lead borate bromine with a KBBF-type structure exhibiting strong nonlinear optical response, *Inorg. Chem. Front.*, 2018, **5**, 916–921.

57 H. Yu, N. Z. Koocher, J. M. Rondinelli and P. S. Halasyamani, Pb$_2$BO$_3$I: A Borate Iodide with the Largest Second-Harmonic Generation (SHG) Response in the KBe2BO3F2 (KBBF) Family of Nonlinear Optical (NLO) Materials, *Angew. Chem., Int. Ed.*, 2018, **57**, 6100–6103.

58 G. Zou, Z. Ma, K. Wu and N. Ye, Cadmium-rare earth oxyborates Cd$_4$ReO(BO$_3$)$_3$ (Re = Y, Gd, Lu): congruently melting compounds with large SHG responses, *J. Mater. Chem.*, 2012, **22**, 19911–19918.

59 M. Luo, C. Lin, G. Zou, N. Ye and W. Cheng, Sodium-rare earth carbonates with shorite structure and large second harmonic generation response, *CrystEngComm*, 2014, **16**, 4414–4421.

60 G. Zou, L. Huang, N. Ye, C. Lin, W. Cheng and H. Huang, CsPbCO$_3$F: A Strong Second-Harmonic Generation Material Derived from Enhancement via p-pi Interaction, *J. Am. Chem. Soc.*, 2013, **135**, 18560–18566.

61 G. Yang, G. Peng, N. Ye, J. Wang, M. Luo, T. Yan and Y. Zhou, Structural Modulation of Anionic Group Architectures by Cations to Optimize SHG Effects: A Facile Route to New NLO Materials in the ATCO$_3$F (A = K, Rb; T = Zn, Cd) Series, *Chem. Mater.*, 2015, **27**, 7520–7530.

62 G. Zou, C. Lin, H. G. Kim, H. Jo and K. M. Ok, Rb$_2$Na (NO$_3$)$_3$: A Congruently Melting UV-NLO Crystal with a Very Strong Second-Harmonic Generation Response, *Crystals*, 2016, **6**, 42.

63 S. Zhao, Y. Yang, Y. Shen, B. Zhao, L. Li, C. Ji, Z. Wu, D. Yuan, Z. Lin, M. Hong and J. Luo, Cooperation of Three Chromophores Generates the Water-Resistant Nitrate Nonlinear Optical Material Bi$_3$TeO$_6$OH(NO$_3$)$_2$, *Angew. Chem., Int. Ed.*, 2017, **56**, 540–544.

64 H. Li, G. Li, K. Wu, B. Zhang, Z. Yang and S. Pan, BaB$_2$S$_4$: An Efficient and Air-Stable Thioborate as Infrared Nonlinear Optical Material with High Laser Damage Threshold, *Chem. Mater.*, 2018, **30**, 7428–7432.

65 Y.-Y. Li, B.-X. Li, G. Zhang, L.-J. Zhou, H. Lin, J.-N. Shen, C.-Y. Zhang, L. Chen and L.-M. Wu, Syntheses,

This journal is © the Partner Organisations 2020

Inorg. Chem. Front., 2020, **7**, 839–852 | **851**

Characterization, and Optical Properties of Centrosymmetric $Ba_3(BS_3)_{1.5}(MS_3)_{0.5}$ and Noncentrosymmetric $Ba_3(BQ_3)(SbQ_3)$, *Inorg. Chem.*, 2015, **54**, 4761–4767.

66 Y. Song, M. Luo, F. Liang, N. Ye and Z. Lin, The second-harmonic generation intensification derived from localization conjugated pi-orbitals in O_2^{2-}, *Chem. Commun.*, 2018, **54**, 1445–1448.

67 G. Zou, H. Jo, S.-J. Lim, T.-S. You and K. M. Ok, Rb_3VO $(O_2)_2CO_3$: A Four-in-One Carbonatoperoxovanadate Exhibiting an Extremely Strong Second-Harmonic Generation Response, *Angew. Chem., Int. Ed.*, 2018, **57**, 8619–8622.

68 G. Zou, Z. Lin, H. Zeng, H. Jo, S.-J. Lim, T.-S. You and K. M. Ok, $Cs_3VO(O_2)_2CO_3$: an exceptionally thermostable carbonatoperoxovanadate with an extremely large second-harmonic generation response, *Chem. Sci.*, 2018, **9**, 8957–8961.

69 M. Xia, X. Jiang, Z. Lin and R. Lit, "All-Three-in-One": A New Bismuth-Tellurium-Borate Bi_3TeBO_9 Exhibiting Strong Second Harmonic Generation Response, *J. Am. Chem. Soc.*, 2016, **138**, 14190–14193.

70 C. Li, W. Yin, P. Gong, X. Li, M. Zhou, A. Mar, Z. Lin, J. Yao, Y. Wu and C. Chen, Trigonal Planar $[HgSe_3]^{4-}$ Unit: A New Kind of Basic Functional Group in IR Nonlinear Optical Materials with Large Susceptibility and Physicochemical Stability, *J. Am. Chem. Soc.*, 2016, **138**, 6135–6138.

71 Z. Li, Y. Yang, Y. Guo, W. Xing, X. Luo, Z. Lin, J. Yao and Y. Wu, Broadening Frontiers of Infrared Nonlinear Optical Materials with π-Conjugated Trigonal-Planar Groups, *Chem. Mater.*, 2019, **31**, 1110–1117.

72 K. E. Woo, J. Wang, J. Mark and K. Kovnir, Directing Boron-Phosphorus Bonds in Crystalline Solid: Oxidative Polymerization of P=B=P Monomers into 1D Chains, *J. Am. Chem. Soc.*, 2019, **141**, 13017–13021.

73 P. Gong, S. Zhang, G. Song, X. Liu and Z. Lin, An Unprecedented Planar π-conjugated $[B_2P_5]^{5-}$ Group with Ultralarge Birefringence and Nonlinearity: an ab initio Study, *Chem. Commun.*, 2020, **56**, 643–646.

74 L. Huang, G. Zou, H. Cai, S. Wang, C. Lin and N. Ye, $Sr_2(OH)_3NO_3$: the first nitrate as a deep UV nonlinear optical material with large SHG responses, *J. Mater. Chem. C*, 2015, **3**, 5268–5274.